

## Indigo carmine pigment adsorption utilizing MgO nanostructures fabricated from *pimpinella anisum* extract

N. Y. Elamin<sup>a,b,\*</sup>

<sup>a</sup>Chemistry Department, College of Science, Imam Mohammad Ibn Saud Islamic University (IMSIU), Riyadh 11623, Kingdom of Saudi Arabia

<sup>b</sup>Department of Chemistry, Sudan University of Science and Technology, P.O. Box 407, Khartoum 11111, Sudan

The effectiveness of MgO nanostructures for removing indigo carmine (IC) dye from an aqueous solution is demonstrated in this article. The nanomaterials were synthesized using  $MgCl_2 \cdot 2H_2O$  and NaOH in a medium containing *Pimpinella anisum* extract. The microstructure of the samples was investigated using XRD, SEM, EDX, BET, and FTIR. Additionally, the IC dye uptake and adsorption processes were investigated using a MgO sorbent. To synthesize the MgO1 and MgO2 materials, the adsorption kinetics of IC dye, the starting pH of IC dye solution, and contact time were optimized. The maximal theoretical adsorption efficiency of the MgO1 and MgO2 adsorbents for IC dye was 559.2 and 492.6 mg/g, respectively, according to the Langmuir isotherm adsorption model. Further, recycling the MgO1 adsorbent proved conceivable due to its ease of collection and re-use following five adsorption-regeneration cycles.

(Received March 1, 2022; Accepted July 22, 2022)

**Keywords:** *Pimpinella anisum* extract, MgO nanostructures, IC dye removal, FTIR mechanism, Adsorption, recycling.

### 1. Introduction

Due to the dangers, organic dyes pose to human health and the overall ecosystem, it is critical to find environmentally friendly solutions to remove them [1-3]. Numerous techniques have been discovered to date, including microbial degradation, photodegradation, and membrane filtration. Among them, adsorption is one of the most successful ways for eliminating organic dyes due to its low cost, high efficiency, ease of operation, and reusability. Numerous adsorbents have been designed to remove various organic dyes due to the advancement of nanotechnology [4-6]. Despite these developments, we must develop an abundant, low-cost, and nontoxic adsorbent with a high capacity for adsorption, great stability, and ease of extraction from the liquid [7].

At present, nanomaterials fabricated using green methodologies have assumed tremendous serious importance in various applications of technology in the multidiscipline of science [8-10], owing to their nanomaterials are requesting, individual characteristics, features, and diversity shapes, particles sizes, and surface properties [11, 12]. Metals oxide nanoparticles are constructed from numerous approaches such as the sol-gel method [13], Hydrothermal procedure [14], co-precipitation [15], ball milling process [16]; besides, several capable devices are developed depending on nanotechnology, including the advantages of safety, adaptability, and eco-friendly environment and these are uncomplicated, inexpensive cost, great purity with high surface area, and display unique physicochemical characteristics [17, 18].

MgO nanocrystalline possesses achieved developed interest for multiple domains of physical and chemical applications. In addition, MgO is becoming a competitor for environmental applications as an adsorbent for water treatment [19, 20]. According to the increased surface area,

\* Corresponding author: nyelamin@imamu.edu.sa

tiny particle sizes serve convenience as an adsorbent of organic dyes in an aqueous solution [21, 22].

This study generated MgO nanostructures sorbent applying the green technique in *Pimpinella anisum* seeds extract at ambient temperature. Prepared MgO sorbent has been utilized to treat and eradicate different dangerous organic dyes. The applicability of the starting concentration, pH, and connecting time toward the sorption capacity has been evaluated. Besides, the adsorption isotherms, kinetic investigations, and recyclability ability also have been presented. FTIR study has identified a viable technique for eliminating IC dye on the MgO surface.

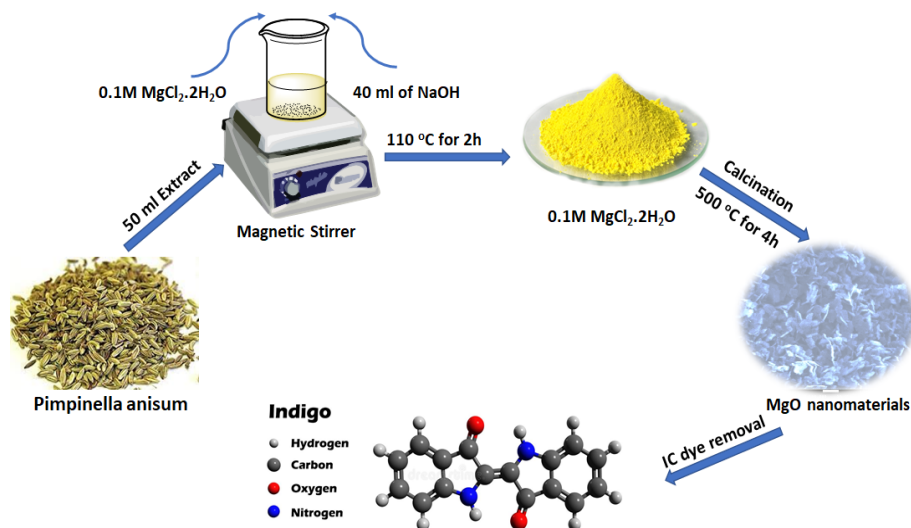
## 2. Experimental methods

### 2.1. Preparation of *Pimpinella anisum* extract

The seeds of *Pimpinella anisum* were thoroughly cleaned with running tap water to remove dust particles, and then with distilled water. An extract was prepared by mixing 5 g of seeds along with 100 mL of distilled water in a 250 mL glass beaker. After 5 minutes of boiling, the mixture became brown yellow in color. Afterwards, the mixture was cooled to room temperature, and filter paper Whatman No. 1 was used. For further experimentation, the extract was kept at room temperature.

### 2.2 Synthesis of magnesium oxide nanoparticles

The purified magnesium oxide nano powders were made using Magnesium Chloride dihydrate ( $\text{MgCl}_2 \cdot 2\text{H}_2\text{O}$ ), sodium hydroxide (NaOH) and extract of *Pimpinella anisum*. 0.1M of  $\text{MgCl}_2 \cdot 2\text{H}_2\text{O}$  is dissolved in 100 mL of distilled water in a 250-mL beaker. The mixed solution is heated to 75 °C with constant stirring, and then 50 ml of *Pimpinella anisum* extract is added to the mixture of Magnesium Chloride dehydrate solution. A sodium hydroxide pellet (8M) is mixed with 40 mL of distilled water and added to a solution in a burette dropwise. A transition from light yellow to dark yellow was observed immediately in the solution. Suddenly, the precipitate turns dark yellow. Using distilled water, the yellow precipitate was washed four times and filtered using Whatman No.1 paper. A two-hour drying procedure was then carried out at 110°C for the washed precipitate. A final calcination at 500°C for four hours was performed on the product. The same experiment was repeated at different concentrations (0.2M) as shown in Scheme 1.



Scheme 1. Arrangement of fabrication MgO nanostructures using *Pimpinella Anisum* extract.

### 2.3. Characterization Techniques

Different techniques have been used to characterize the obtained magnesium oxide nanoparticles. A study of the powder's XRD patterns revealed the phase structure of the MgO nanoparticles and their average size. A diffractometer (D8 Advance Bruker, Mannheim, Germany) was used to record the samples using a Cu-K $\alpha$  radiation ( $\lambda = 0.15406$  nm). A SEM-EDX analysis was performed in order to observe and measure the structural morphology and chemical composition of magnesium oxide nanoparticles. In order to create electrical conduction on the surface of MgO powder, the specimens were oven-dried at 105 °C and coated with a thin layer of gold. FTIR (Nicolet 6700, Thermo Fisher, Waltham, MA, USA) was carried out to determine the chemical bonding mode in the prepared samples in the range of 4000–400 cm<sup>-1</sup> with a resolution of 4 cm<sup>-1</sup>. The optical properties of MgO NPs were examined using UV-Vis (Shimadzu UV-Vis 2450). Nitrogen adsorption-desorption isotherms at the boiling point (77 K) of N<sub>2</sub> were used to estimate Brunauer, Emmett and Teller specific surface area (BET SSA) and average pore diameter and volume. To remove moisture and adsorbed impurities, the sample was degassed at 200 °C under He gas flow for 2 hours before the adsorption experiment. Brunauer, Emmett, and Teller (BET) model and t-plot scheme by Lippens and de Boer were used to estimate the specific surface area and porosity.

### 2.4. Kinetic adsorption of IC dye procedure

Kinetic adsorption was carried out using 500ml of IC solution at a fixed concentration of 20mg/L. To IC, 100 mg of the composite was added and stirred in darkness for 2 hours. After being withdrawn at 1, 2, 5, 10, 15, 20, 30, 45, 60, 90, 120, 150 and 180min, a nylon membrane-syringe filter (0.2\* $\mu$ m) was applied, centrifuged, and then filtered. The remaining concentration was then measured using a spectrophotometer (Labomed - UVS-2800) at 611 nm Lambda-max. Equation (1) can be used to calculate the amount of IC adsorbed per gram of nanomaterials at time (min).

$$q_t = \frac{V(C_0 - C_t)}{m} \quad (1)$$

With the following formula,  $q_t$  is defined as the adsorbed quantity of IC per gram of IC at time  $t$ ,  $C_0$  is the initial concentration of IC,  $C_t$  the concentration of IC at time  $t$ ,  $v$  the volume of the solution (mL) and ( $m$ ) the mass of the sorbent used (mg):

$$q_t = \frac{V(C_0 - C_t)}{m} \quad (2)$$

## 3. Results and discussion

### 3.1. Structural analysis

The crystalline structure of MgO nanoparticles was determined by X-Ray diffraction. Fig. 1 shows the XRD pattern of synthesized MgO nanoparticles at different concentration (0.1M and 0.2M). The existence of strong and sharp peaks located at the  $2\theta$  value which are corresponding to (1 1 1), (0 0 2) and (0 2 2), (1 1 3) and (2 2 2) planes respectively indicated diffraction the formation of MgO nanoparticles. The intense and sharp peaks indicate that the obtained products are well-crystallized. The intensity of the peaks resulting from the concentration 0.1M is greater than that resulted from the 0.2M. The diffraction peaks of MgO can be matched with JCPDS card no. 450946 [23]. The XRD patterns also confirm significant changes in the crystallite size with the increase in concentration. The average crystallite size was calculated using Debye-Scherrer's equation [24].

$$D = \frac{k\lambda}{\beta \cos \theta} \quad (3)$$

$d$ -spacing values were obtained from Bragg's equation as follows [25]:

$$d = \frac{\lambda}{2 \sin \theta} \quad (4)$$

where  $D$  is the average crystallite size in Å,  $k$  is the shape factor (0.9),  $\lambda$  is the wavelength of X-ray (1.5406 Å),  $\theta$  is the Bragg angle. By applying Scherrer's equation, the average crystallite size is found to increase with molarity concentrations. The average crystallite sizes of MgO1 and MgO2 samples were 7.92 nm and 9.56 nm, with  $d$ -spacing of 2.10 and 2.11, respectively.

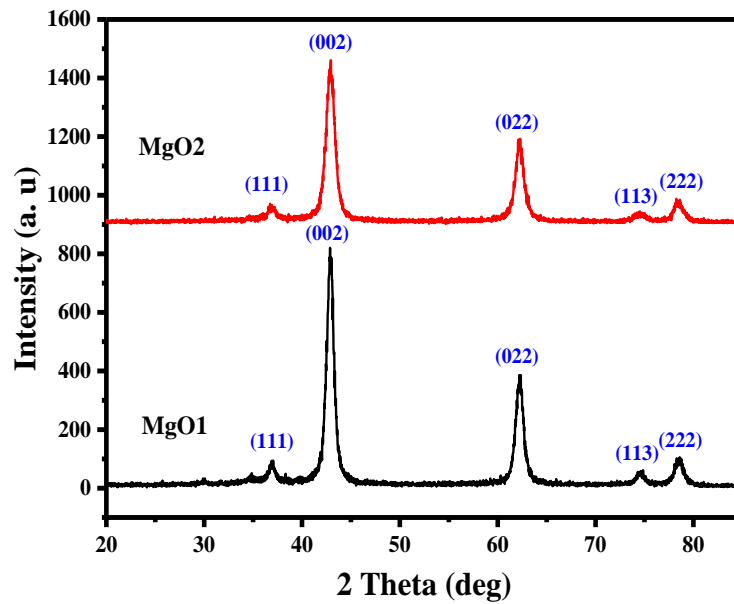


Fig. 1. XRD diffraction patterns of MgO1 and MgO2 nanostructures.

### 3.2. SEM analysis of nanostructures samples

Fig. 2 shows the SEM images of MgO nanoparticles which were prepared in different concentrations. The structure, morphology and size of MgO nanoparticles was investigated by SEM. It was observed that the average size of MgO1 particles is smaller than MgO2. The size of the MgO particles calculated from SEM micrographs agree well with those obtained using X-ray diffraction.

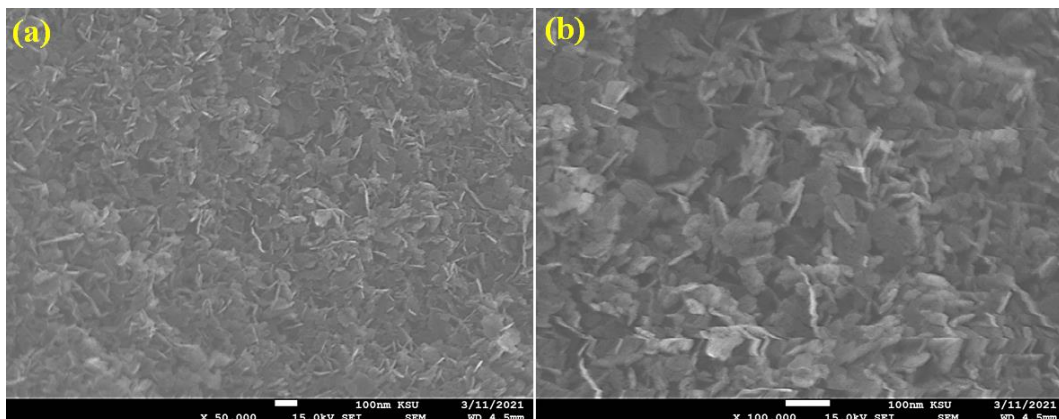


Fig. 2. SEM image of MgO sample (a) MgO1 (b) MgO2.

### 3.3. EDX analysis

Energy dispersive X-ray spectroscopy (EDX) is obtained and evaluated for quantitative and qualitative determinations of the elements as shown in Fig. 3a and b. It demonstrated the chemical composition of the synthesized nanoparticles and confirm the presence of MgO1 nanoparticles. In EDX spectra of MgO1 nanoparticles, two separate strong signals were observed which confirm that the grown nanoparticles are composed of Magnesium and oxygen only without any impurity of peaks. Hence, nanoparticles are obtained in pure forms with molecular ratio 1:1 for Mg and O respectively. A brighter zone on the elemental map implies a significant concentration of that element. Elements Mg and O are equally distributed across all examined particles, indicating that homogenous MgO1 nanostructures were successfully synthesized as shown in Fig. 3c and d.

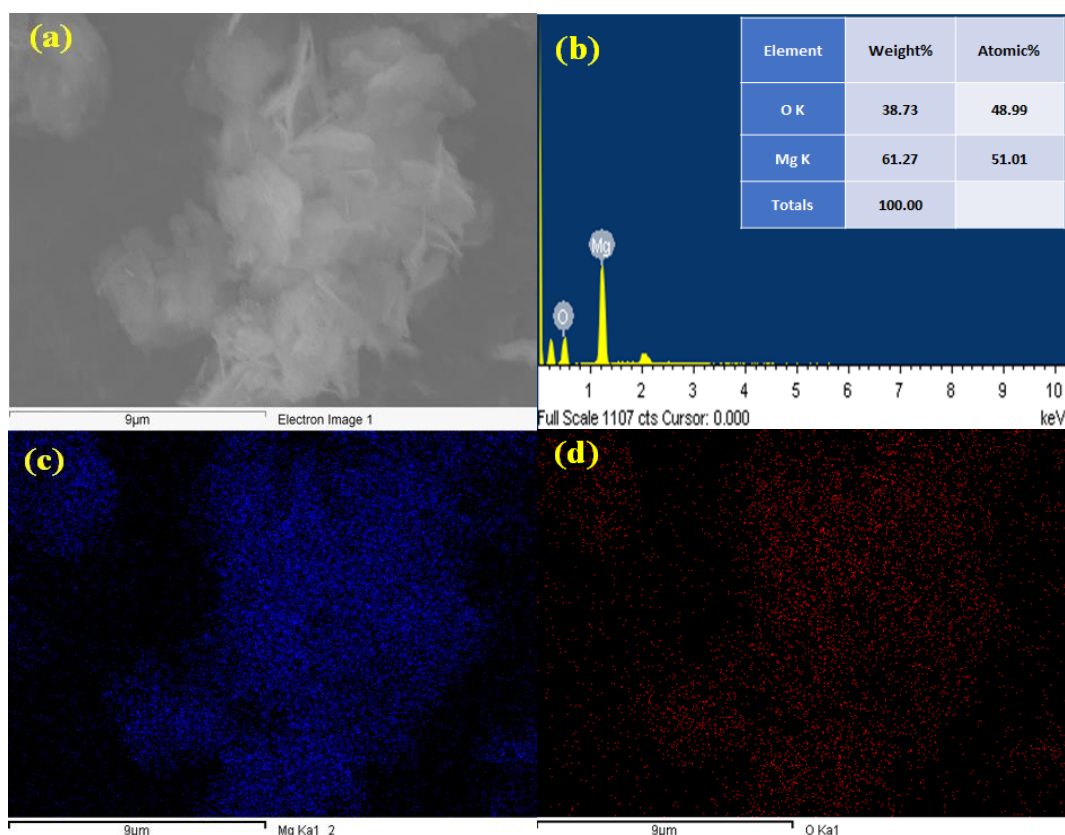


Fig. 3. (a-d). EDX spectrum of MgO1 nanoparticles.

### 3.4. Surface area analysis (BET)

One of the first indicators to identify whether a material or product contains nano and thus is potentially entitled as a nanomaterial is its specific surface area. The surface texture properties of MgO1 and MgO2 were measured employing Brunauer Emmett Teller analyzer (BET) along with the Barrett Joyner Halenda (BJH) diagram. Nitrogen adsorption is used to measure the specific surface area of a powder. The result obtained from the N<sub>2</sub> sorption isotherm confirmed that the isotherm is Langmuir type IV (Fig. 4a) with relative pressure ( $P/P_o = 0.1 - 0.99$ ). Besides, the hysteresis loop is type H3 (Fig. 4b), which confirms the mesoporous characteristic of the nanoparticles with slit-shaped pores. The specific surface area of the particles of MgO1 is  $127.442 \text{ m}^2 \cdot \text{g}^{-1}$ , Furthermore, the pore size distribution and pore volume are  $16.995 \text{ \AA}$  and  $0.8 \text{ cm}^3 \cdot \text{g}^{-1}$ , while its  $106.304 \text{ m}^2 \cdot \text{g}^{-1}$ ,  $18.204 \text{ \AA}$  and  $0.868 \text{ cm}^3 \cdot \text{g}^{-1}$  respectively for MgO2. Therefore, MgO1 nanoparticles exhibit a relatively high surface area per unit mass compared to MgO2, so MgO1 gives better adsorption properties than MgO2.

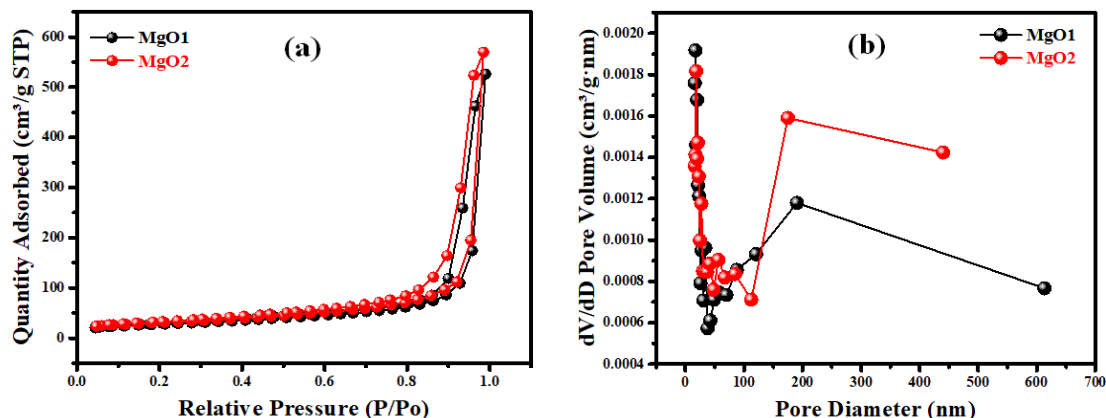


Fig. 4. (a)  $N_2$  adsorption –desorption isotherm (BET) and (b) (BJH) pore size distribution of the MgO nanoparticles samples.

### 3.5. FTIR Study and Purity

The formation and purity of MgO1 nanoparticles were investigated employing FTIR spectroscopy in the range of  $400\text{--}4000\text{ cm}^{-1}$ . FTIR spectrum of MgO1 nanoparticles synthesized at different molarities are shown in Fig. 5. The FTIR spectra for MgO nanoparticles show vibration peaks at  $3434$  and  $3438\text{ cm}^{-1}$  which are attributed to the O–H stretching of water molecules on the surface of the MgO [26]. Peaks at  $1625$  and  $1633\text{ cm}^{-1}$  are attributed to the bending vibration of water molecule, which may be caused by the absorption of moisture during measurements [27, 28]. The Mg–O bond stretching peaks at  $420$  and  $434\text{ cm}^{-1}$  indicate that the prepared nanomaterials are of high purity [21, 29].

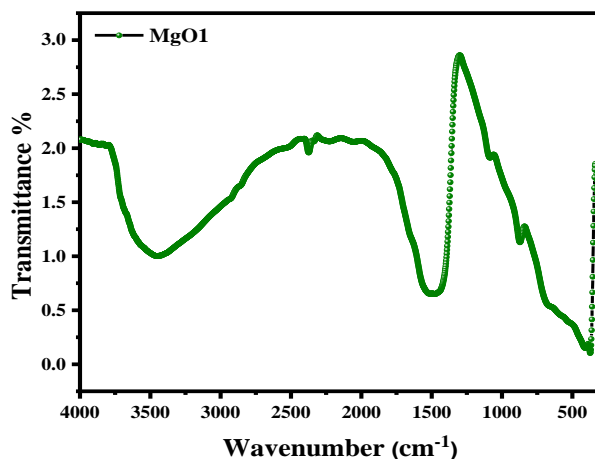


Fig. 5. FTIR spectra of MgO1 nanoparticles at different concentration.

### 3.6. IC dye adsorption on MgO nanoparticles studies

#### 3.6.1. Equilibrium contacts time

In this study, the effect of equilibrium time (contact time) on the adsorption of IC dye on MgO1 and MgO2 sorbents was investigated further. Because of the rapid removal rate observed within the first few minutes of contact time (20 min and 40 min utilizing MgO1 and MgO2 for eliminating IC dye in both), the equilibrium period was reached reasonably quickly. As shown in Fig. 6, the removal efficiencies were extremely rapid during the first few minutes of contact (20 min and 40 min using MgO1 and MgO2 for removing IC dye, respectively). The obtained results confirmed that the IC dye removal capacity increased quickly and reached equilibrium, as

demonstrated in Fig. 6. The rapid equalization velocity is caused by the electrostatic interactions of adsorption sites on the MgO1 and MgO2 surfaces and the dye. Furthermore, because of the high specific surface area of the MgO1, it was easy for the MgO1 to come into touch with the organic dye contaminants. IC dye sorption on MgO1 was seen to be beyond the surface at the time of opening contact, which was attributed to the larger surface area and active sides of MgO1 than MgO2 following the IC sorption process on MgO2 at the time of opening contact. The adsorption on the outer surface achieved saturation point during this period, and the dye diffused into the adsorbent pores and was absorbed by the inner surface of the MgO adsorbent during the next time. The equilibrium times for IC dye were 20 and 40 minutes, respectively; after that, no further adsorption occurred even after a considerable contact of time.

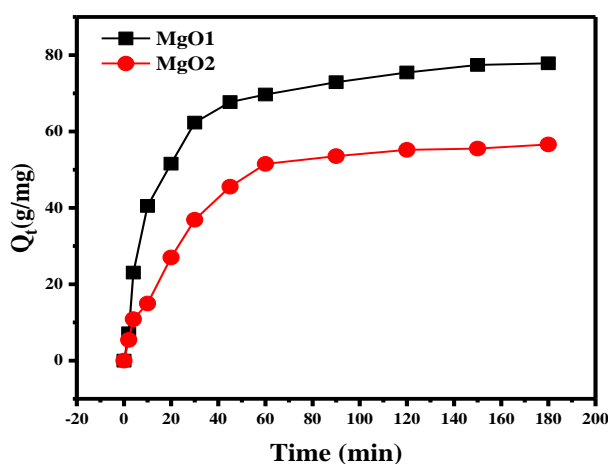


Fig. 6. Contact time equilibrated of IC dye of MgO nanostructures samples.

### 3.6.2. IC dye adsorption kinetics

The removal kinetics of adsorbent materials is the primary criterion for their efficacy. The kinetics of IC dye removal from MgO1 and MgO2 nanomaterials were determined using a standard solution 250 ppm IC dye at ambient temperature and pH neutral. To have a better understanding of the removal mechanism, it is necessary to study adsorption kinetics, which is required for the process's experimentation. As a result, we assessed pseudo-first order (PFO) and pseudo-second order (PSO) kinetics models to determine which one provides the best fit to the experimental observations (Fig 7a-d). The nonlinear model equations and the kinetics values generated from the plots are shown in Table 1. Correlation coefficients ( $R^2$ ) analysis was used to compare the kinetic data fits. The estimated parameters  $k_1$ ,  $k_2$ , and the regression coefficients  $R^2$  were given in Tables 1 based on the slope and intercept of identical regression graphs. The  $R_2$  value obtained from the PSO plots is significantly greater than the  $R_2$  value obtained from the PFO model, indicating that the adsorption process can be more accurately represented. Additionally, the projected removal capacity using the PSO pattern is consistent with the experimental results. These findings indicate that chemisorption controls and manages the adsorption process, and that the interaction between the organic dye sorbate and the MgO1 and MgO2 sorbents involves electron participation [30].

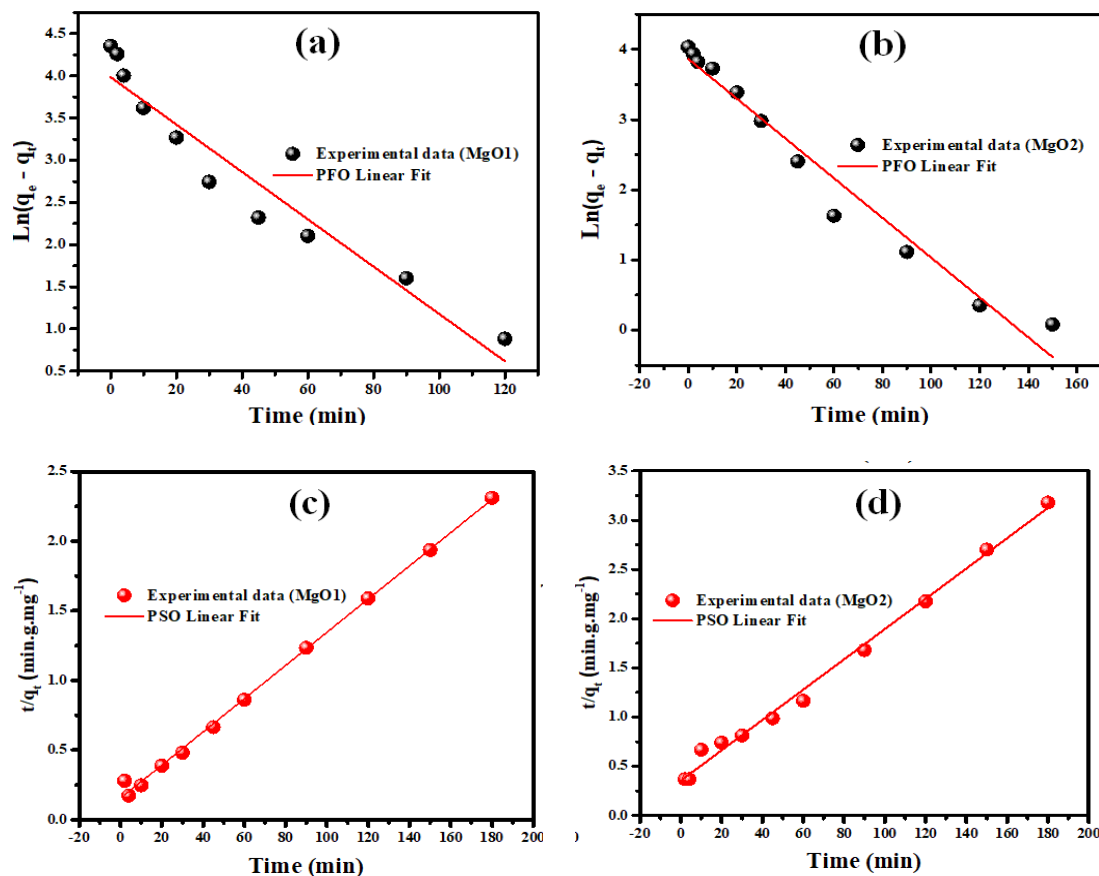


Fig. 7. Pseudo-First-order (PFO) (a) MgO1 and (b) MgO2, Pseudo-Second-order (FSO) (c) MgO1 and (d) MgO2 for IC removal.

Table 1. Kinetics models parameters for the IC dye removal on MgO nanoparticles.

Kinetics Model	Kinetic Equation	Parameter	MgO1	MgO2
Pseudo-first order	$\ln(q_e - q_t) = \ln q_e - k_1 t$ [31]	$q_m$	74.23	56.40
		$K_1$	0.0671	0.0354
		$R^2$	0.9468	0.9698
Pseudo-second order	$\frac{t}{q_t} = \left[ \frac{1}{k_2 q_e^2} \right] + \frac{1}{q_e} t$ [31]	$q_m$ (exp)	83.11	66.98
		$q_m$ (cal)	78.97	59.54
		$K_2$	0.00107	0.00059
		$R^2$	0.9997	0.9986

### 3.6.3. Adsorption isotherms

Because it was necessary to understand the mechanism of removal of the IC dye from the MgO1 and MgO<sub>2</sub> surfaces as well as to assess the greatest adsorption capability manifested through nanostructures that were fabricated for the organic model dye, the adsorption results for IC dye were adopted from widely scrutinized adsorption equilibrium patterns, such as Freundlich and Langmuir. On the following pages are presented the nonlinear formulas for the isotherms. Fig. 8a and b show the results of nonlinear and linear isotherm graphs for IC dye adsorption on nanomaterials, respectively, whereas graphs contain information on the calculated isotherm variables.

In the case of IC dye adsorption into MgO1 and MgO<sub>2</sub>, it can be noted that the findings obtained from the isotherm plots and correlation coefficient ( $R^2$ ) estimates for the adsorption

datum closely resemble the Langmuir and Freundlich isotherm form. Based on the results, it was determined that the Langmuir model for inorganic dye adsorption provides a more satisfactory fit, with regression coefficients  $R^2$  equal to 0.99 and 0.89, which are correlated with  $R^2$  equal to 0.95 and 0.98 for the Freundlich model in that order, respectively. In accordance with the Langmuir isotherm model, the greatest adsorption capacity demonstrated by MgO1 and MgO2 for IC dye is computed to be 559.2 and 492.6 mg. g<sup>-1</sup>, respectively, as depicted in Fig.8 a and c.

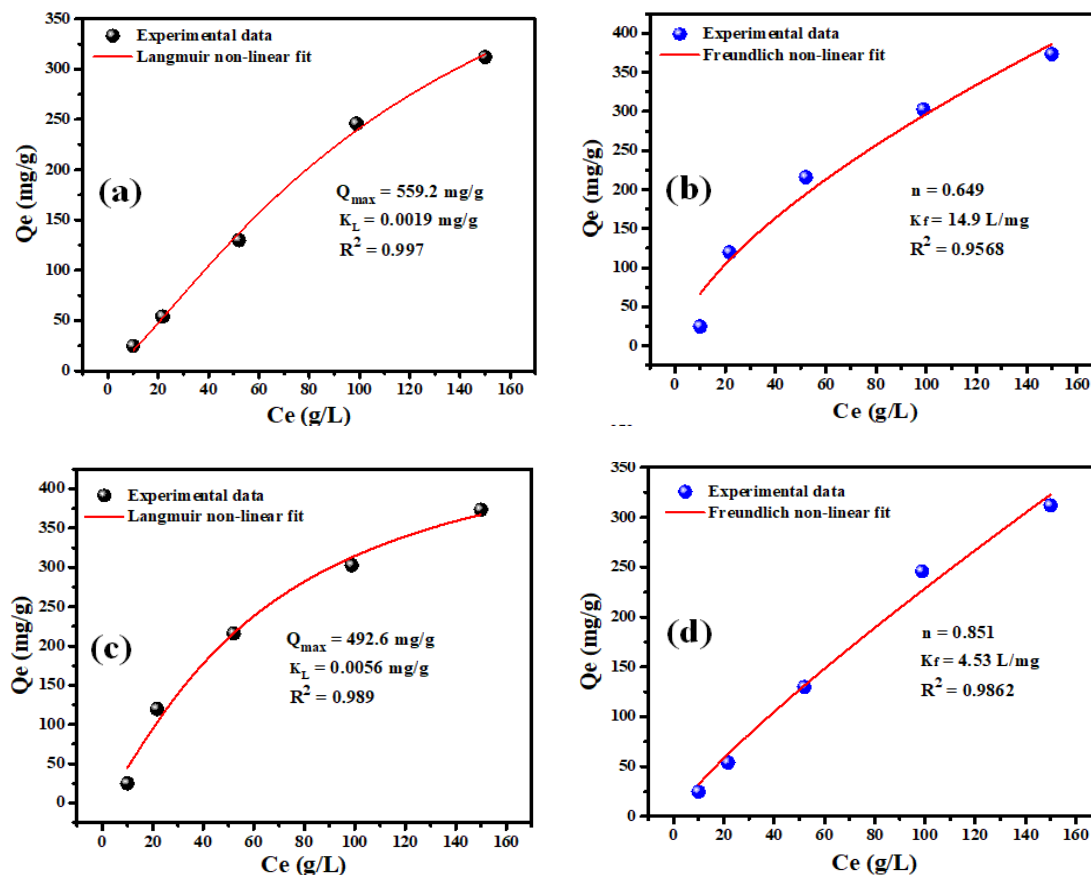


Fig. 8. Assessment of isotherm models (Langmuir and Freundlich) for IC dye adsorption on MgO1 (a) and (b) and MgO2 (c) and (d) in that order.

### 3.6.4. Dependence of variation pH on IC dye adsorption

The pH value is a critical factor impacting the adsorbent's surface characteristics and the availability of appropriate functional groups on the adsorbate molecules [2, 32]. The adsorbent and adsorbate molecules often contain a variety of surface functional groups that can be protonated/deprotonated in response to the medium pH, so modulating the electrostatic interaction between opposite charges and thereby increasing the effectiveness of pollutant removal. Indigo Carmine has a pKa of 12.6 (-N-H group); as a result, its structure remains constant at lower pH values, and it is negatively charged over a large pH range [33]. Fig. 9 illustrates the effect of altering the pH of IC dye solutions in the range of 2.0 to 11.0 on the removal efficiency. The data indicated slightly larger adsorption capacities were obtained at pH values less than 7.0, which is below the solid MgO1  $pH_{ZC} = 9.2$ . This result could be explained by the strong electrostatic affinity between positively charged MgO1 nanoparticles and negatively charged IC molecules. At pH values greater than 9.2, the dye removal rate reduced partially due to gradual depletion of positive charges on the MgO1 surface and partly due to competition for interaction with the adsorbent surface by the medium OH<sup>-</sup> and the IC dye.

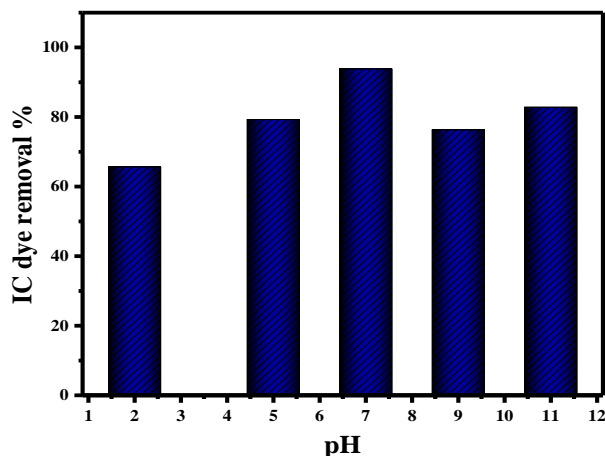


Fig. 9. Impact of pH variation on IC dye removal %.

### 3.6.5. IC dye adsorption mechanism

For adsorption investigations, the primary difficulty is to provide a mechanism that will better understand all conceivable reactions/interactions that occur during the adsorbent surface. In this context, the FTIR technique has been shown to play a critical role in the adsorption process. Thus, several factors must be considered, including but not limited to the adsorbate structure's complex nature, the presence of binding sites, the adsorbent's nanostructure (particle size, shape, porosity, agglomeration level), and surface characteristics (charge, accessible sites), in furthermore to the adsorbent/adsorbate various interactions. The FT-IR spectra of pure IC has many absorption bands in the mid-IR region; the absorption bands at,  $1636\text{ cm}^{-1}$  have been ascribed to the C=O stretching vibration occurring in the IC [34]. The assessment of the MgO1 IR-spectra after IC dye adsorption (Fig. 10) illustrates the appearance of additional peaks associated with the vibration of the IC dye molecule's functional groups (broad bands at  $3200\text{--}3600\text{ cm}^{-1}$ ), as well as hydroxyl groups (broad bands at  $3200\text{--}3600\text{ cm}^{-1}$ ), confirming the IC dye adsorption on the MgO1 surface. Additionally, the free MgO1 peak at  $378\text{ cm}^{-1}$  was moved to a lower value of  $371\text{ cm}^{-1}$ , as shown in Fig 10. The peaks at approximately  $1620$  and  $1452\text{ cm}^{-1}$  are intrinsic to the IC dye. At  $1046\text{ cm}^{-1}$  and  $1338\text{ cm}^{-1}$ , the asymmetric stretching vibration of the S-O bond in the  $\text{SO}_3\text{-H}$  group occurs. The dye adsorption process involves van der Waals interaction and the creation of hydrogen bonds between the functional groups ( $-\text{NH}_2$ ,  $-\text{OH}$ ,  $-\text{SO}_3\text{H}$ ) of the IC structure and the active centers of MgO1 nanostructures.

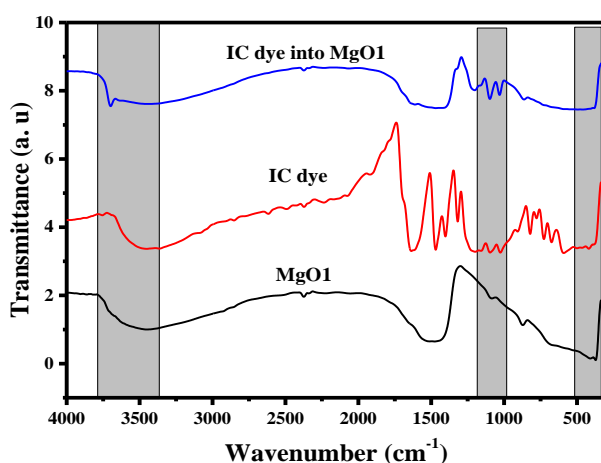


Fig. 10. (a) FTIR spectra of MgO1, IC dye and MgO1@IC.

### 3.6.6. MgO1 nanoparticle recyclability and generation

The scaling up and industrial applications, the reusability, and regeneration of an adsorbent (MgO1) are important considerations. Therefore, it's important to test MgO1's cyclic viability before proceeding. In order to recover the MgO1 nanoparticles utilized in the sorption experiment, filtering was performed followed by calcination at 500°C for one hour. Later, the MgO1 that had been collected was re-used in additional adsorption experiments. In the reusability performance trial, as shown in Fig. 11, it can be shown that MgO1 is effective for the removal of IC dye for at least three recycles, with a mean value of around 91%.

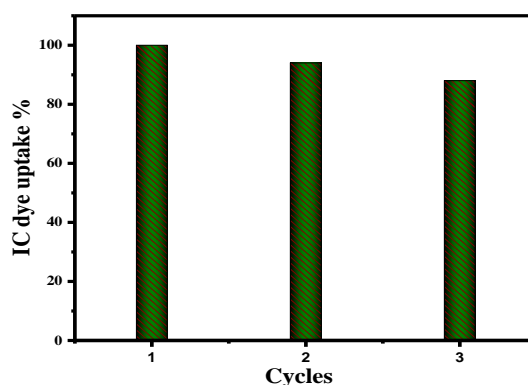


Fig. 11. Reusability and recyclability Effectiveness.

To verify MgO's adsorption properties for IC pigment, the obtained results are compared to those reported in the literature for those other adsorbent materials, as shown in Table 2. It is obvious that MgO nanostructures function exceptionally well in removing IC dye, with an adsorption capacity of 559.2 mg. g<sup>-1</sup> and an adsorption rate ( $k_2$ ) of 0.00107 g/mg/min.

Table 2. Comparisons IC dye removal abilities with previous designated adsorbent nanomaterials.

Adsorbent Used	PSO Model		Langmuir Model		Optimum pH	Ref
	$k_2$ (g/mg/min)	$R^2$	$q_m$ (mg/g)	$R^2$		
GO/PANI nanocomposite	0.01090	0.999	88.73	0.992	2.0	[35]
Coagulation flocculation	0.00200	0.986	29.54	0.970	7.0	[36]
Terminalia catappa shell	0.01350	1.000	50.50	0.987	2.0	[37]
Carboxymethyl Chitosan	0.00013	0.995	130.5	0.982	3.0	[38]
Activated carbon	0.21900	0.995	30.00	1.000	4.0	[39]
<b>MgO1 nano-adsorbent</b>	<b>0.00107</b>	<b>0.9997</b>	<b>559.2</b>	<b>0.997</b>	<b>7.0</b>	<b>This paper</b>

## 4. Conclusion

In conclusion, we have devised a green and sustainable process for fabricating MgO nanostructures with varying surface areas, which demonstrated good adsorption characteristics for organic dyes when tested (IC). Utilizing FTIR, it was determined that the electrostatic force, hydrogen bonding interaction, and hydrophobic interaction between the MgO surface and the IC dye were all present. The equilibrium isotherm models, and kinetic fitting were employed for the mechanism investigation, which validated the adsorption mechanisms of the MgO nanoparticles even more strongly than previously thought. Also investigated was the effect of pH variations on the adsorption of indigo dye from aquatic media. Because of this, the synthesis of MgO nanostructures to remediate contaminated drinking water tainted by organic and inorganic pollutants seems to promise.

## References

1. Modwi, A., et al., Environmental Research, 2022. 205: p. 112543;  
<https://doi.org/10.1016/j.envres.2021.112543>
- [2] Aissa, B., et al., International Journal of Environmental Science and Technology, 2021: p. 1-14.
- [3] Kerrami, A., et al., Environmental Science and Pollution Research, 2021. 28(41): p. 57543-57556; <https://doi.org/10.1007/s11356-021-14682-z>
- [4] Toghan, A. and A. Modwi, Journal of Photochemistry and Photobiology A: Chemistry, 2021. 419: p. 113467; <https://doi.org/10.1016/j.jphotochem.2021.113467>
- [5] Toghan, A., et al., Diamond and Related Materials, 2021. 118: p. 108491;  
<https://doi.org/10.1016/j.diamond.2021.108491>
- [6] Rahali, S., et al., Langmuir, 2021. 37(24): p. 7285-7294;  
<https://doi.org/10.1021/acs.langmuir.1c00378>
- [7] Abdulkhair, B.Y., et al., Zeitschrift für Naturforschung A, 2019. 74(10): p. 937-944;  
<https://doi.org/10.1515/zna-2019-0059>
- [8] Manjunatha, K., et al., Sensors International, 2021: p. 100127;  
<https://doi.org/10.1016/j.sintl.2021.100127>
- [9] Laurent, S., et al., Chemical reviews, 2008. 108(6): p. 2064-2110;  
<https://doi.org/10.1021/cr068445e>
- [10] Toghan, A., et al., Chemical Physics, 2021. 551: p. 111350;  
<https://doi.org/10.1016/j.chemphys.2021.111350>
- [11] Salih, M., et al., Zeitschrift für Naturforschung A, 2021. 76(9): p. 835-846;  
<https://doi.org/10.1515/zna-2021-0061>
- [12] Modwi, A., et al., Zeitschrift für Naturforschung A, 2021. 76(6): p. 535-547;  
<https://doi.org/10.1515/zna-2021-0009>
- [13] Modwi, A., et al., Journal of Materials Science: Materials in Electronics, 2016. 27(12): p. 12974-12984; <https://doi.org/10.1007/s10854-016-5436-y>
- [14] Bhargava, R. and S. Khan, Physics Letters A, 2019. 383(14): p. 1671-1676;  
<https://doi.org/10.1016/j.physleta.2019.02.030>
- [15] Rahali, S., et al., Langmuir, 2021; <https://doi.org/10.1021/acs.langmuir.1c00378>
- [16] Modwi, A., et al., Journal of Materials Science: Materials in Electronics, 2021. 32(3): p. 3415-3430; <https://doi.org/10.1007/s10854-020-05088-7>
- [17] Manjunathaa, J.G., et al., Advanced Materials Research. 2014. Trans Tech Publ.;  
<https://doi.org/10.4028/www.scientific.net/AMR.895.447>
- [18] Wojcieszak, R., et al., Studies in Surface Science and Catalysis. 2010, Elsevier. p. 789-792;  
[https://doi.org/10.1016/S0167-2991\(10\)75161-2](https://doi.org/10.1016/S0167-2991(10)75161-2)
- [19] Salem, A.-N.M., M. Ahmed, and M. El-Shahat, Journal of Molecular Liquids, 2016. 219: p. 780-788; <https://doi.org/10.1016/j.molliq.2016.03.084>
- [20] Venkatesha, T., et al., Chemical engineering journal, 2012. 198: p. 1-10;  
<https://doi.org/10.1016/j.cej.2012.05.071>
- [21] Modwi, A., et al., Zeitschrift für Naturforschung A, 2018. 73(11): p. 975-983;  
<https://doi.org/10.1515/zna-2018-0219>
- [22] Priyadarshini, B., T. Patra, and T.R. Sahoo, Journal of Magnesium and Alloys, 2021. 9(2): p. 478-488; <https://doi.org/10.1016/j.jma.2020.09.004>
- [23] Athar, T., A. Hakeem, and W.J.A.S.L. Ahmed, Synthesis of MgO nanopowder via non aqueous sol-gel method. 2012. 7(1): p. 27-29; <https://doi.org/10.1166/asl.2012.2190>
- [24] Holzwarth, U. and N.J.N.n. Gibson, The Scherrer equation versus the 'Debye-Scherrer equation'. 2011. 6(9): p. 534-534; <https://doi.org/10.1038/nnano.2011.145>
- [25] Ismail, M., et al., ZnO nanoparticles: Surface and X-ray profile analysis. 2018. 14: p. 381-393.

- [26] Kandiban, M., P. Vigneshwaran, and I.V. Potheher, Synthesis and characterization of mgo nanoparticles for photocatalytic applications. in Proceedings of the National Conference on Advances in Crystal Growth and Nanotechnology. 2015.
- [27] Qiu, L., et al., Composite Structures, 2003. 62(3-4): p. 391-395;  
<https://doi.org/10.1016/j.compstruct.2003.09.010>
- [28] Niu, H., et al., Journal of Nanoparticle Research, 2006. 8(6): p. 881-888;  
<https://doi.org/10.1007/s11051-006-9138-x>
- [29] Bekhti, H., et al., Vibrational Spectroscopy, 2021. 117: p. 103313;  
<https://doi.org/10.1016/j.vibspec.2021.103313>
- [30] Wei, S. and A.R. Kamali, Journal of Alloys and Compounds, 2021. 886: p. 161201;  
<https://doi.org/10.1016/j.jallcom.2021.161201>
- [31] Lagergren, S.K., About the theory of so-called adsorption of soluble substances. Sven. Vetenskapsakad. Handlingar, 1898. 24: p. 1-39.
- [32] Adel, M., M.A. Ahmed, and A.A. Mohamed Monitoring & Management, 2021. 16: p. 100550; <https://doi.org/10.1016/j.enmm.2021.100550>
- [33] Palma-Goyes, R.E., et al., Electrochimica acta, 2014. 140: p. 427-433;  
<https://doi.org/10.1016/j.electacta.2014.06.096>
- [34] Kumari, N. and M. Datta, AInternational Journal of Environment, Ecology, Family and Urban Studies, 2016. 6(5): p. 7-16.
- [35] Gemeay, A.H., R.G. Elsharkawy, and E.F. Aboelfetoh, Journal of Polymers and the Environment, 2018. 26(2): p. 655-669; <https://doi.org/10.1007/s10924-017-0947-z>
- [36] Othmani, A., A. Kesraoui, and M. Seffen, Euro-Mediterranean Journal for Environmental Integration, 2017. 2(1): p. 1-12; <https://doi.org/10.1007/s41207-017-0016-y>
- [37] Zein, R., et al., Biomass Conversion and Biorefinery, 2022: p. 1-18;  
<https://doi.org/10.1007/s13399-021-02290-3>
- [38] Emik, S., S. Işık, and E. Yıldırım, Journal of Polymers and the Environment, 2021. 29(6): p. 1963-1977; <https://doi.org/10.1007/s10924-020-02016-y>
- [39] Sikdar, D., S. Goswami, and P. Das, Biomass Conversion and Biorefinery, 2021: p. 1-13;  
<https://doi.org/10.1007/s13399-021-01385-1>